

**Fluorine donors and  $\text{Ti}^{3+}$  ions in  $\text{TiO}_2$  crystals**

Shan Yang (杨山) and L. E. Halliburton\*

*Physics Department, West Virginia University, Morgantown, West Virginia 26506, USA*

(Received 17 September 2009; revised manuscript received 28 November 2009; published 15 January 2010)

Electron paramagnetic resonance (EPR) and electron-nuclear double resonance (ENDOR) are used to identify and characterize neutral fluorine donors in  $\text{TiO}_2$  crystals having the rutile structure. The fluorine ions substitute for oxygen and are present as unintentional impurities. Isolated singly ionized fluorine donors in an as-grown (fully oxidized) crystal convert to their neutral charge state during exposure to 442 nm laser light at 6 K. These donors return to the singly ionized charge state within a few seconds when the light is removed. In contrast, the neutral fluorine donors are observed at 6 K without photoexcitation after a crystal is reduced at 600 °C in flowing nitrogen gas. The angular dependences of the EPR and ENDOR spectra provide a complete set of spin-Hamiltonian parameters (principal values are 1.9746, 1.9782, and 1.9430 for the  $g$  matrix and  $-0.23$ ,  $0.47$ , and  $5.15$  MHz for the  $^{19}\text{F}$  hyperfine matrix). These matrices suggest that the unpaired electron is localized primarily on one of the two equivalent neighboring substitutional titanium ions, i.e., the ground state of the neutral fluorine donor in rutile-structured  $\text{TiO}_2$  is a  $\text{Ti}^{3+}$  ion adjacent to a  $\text{F}^-$  ion.

DOI: [10.1103/PhysRevB.81.035204](https://doi.org/10.1103/PhysRevB.81.035204)

PACS number(s): 77.84.Bw, 71.55.Ht, 76.30.Mi, 76.70.Dx

**I. INTRODUCTION**

Titanium dioxide ( $\text{TiO}_2$ ) is a versatile wide-band-gap semiconductor with applications ranging from solar energy conversion to self-cleaning hygienic surfaces.<sup>1–6</sup> A strategy presently being used to optimize  $\text{TiO}_2$  for specific applications involves modification of the optical and electrical properties of this material by adding or removing selected donors and acceptors (impurities as well as native defects). Success in these efforts, however, requires a complete understanding of the fundamental characteristics of the donors and acceptors in  $\text{TiO}_2$ , including their electronic structure and optical responses. Although much of the recent experimental work in  $\text{TiO}_2$  has focused on powders, thin films, nanoparticles, nanotubes, nanowires, etc., it is more informative to use bulk crystals to initially and fully investigate the point defects. Electron paramagnetic resonance (EPR) and electron-nuclear double-resonance (ENDOR) techniques are well suited to study paramagnetic point defects in bulk crystals.<sup>7</sup> Information obtained from a bulk crystal can then be used to interpret the EPR spectra observed in various  $\text{TiO}_2$  powders and nanostructures. We have recently used this approach to study the photoinduced paramagnetic charge states of oxygen vacancies in  $\text{TiO}_2$  (rutile) crystals.<sup>8</sup> An important result of our earlier work was to show experimentally that the ground state of the neutral oxygen vacancy is magnetic (i.e., the neutral oxygen vacancy has  $S=1$ ). The two electrons trapped at the vacancy are localized on two of the three neighboring titanium ions and are coupled ferromagnetically.<sup>8</sup> These observations may help explain the ferromagnetic behavior reported in recent studies of  $\text{TiO}_2$ .<sup>9–11</sup>

In the present paper, EPR and ENDOR are used to determine the electronic structure of the neutral fluorine donor in single crystals of  $\text{TiO}_2$ . Fluorine ions substitute for oxygen ions in this lattice<sup>12–15</sup> and act as shallow donors. In a fully oxidized sample, these isolated fluorine donors are initially in the singly ionized charge state (with no unpaired electrons to give an EPR signal). At low temperature, 442 nm laser light populates the neutral charge state (thus producing an

$S=1/2$  EPR signal). This EPR signal in a fully oxidized sample quickly decays at low temperature after removing the light when self-trapped holes thermally release and recombine with the electrons at the neutral fluorine donors. In contrast, the neutral fluorine donor EPR signal is present at low temperature without photoexcitation in a sample that has been reduced at high temperature. The principal values and directions of the principal axes for the  $g$  matrix and the  $^{19}\text{F}$  hyperfine matrix are obtained from the angular dependences of the EPR and ENDOR spectra. A model consisting of a substitutional  $\text{Ti}^{3+}$  ion adjacent to a substitutional  $\text{F}^-$  ion is established for the ground state of the neutral fluorine donor in  $\text{TiO}_2$ , i.e., the unpaired spin is localized primarily on a neighboring titanium ion instead of being centered on the fluorine ion.

**II. EXPERIMENTAL**

The  $\text{TiO}_2$  crystals used in this investigation have the rutile structure and were purchased from MTI Corporation (Richmond, CA). They were grown by the four-mirror floating-zone method. Three EPR-sized samples for this study, one with dimensions of  $3 \times 5 \times 1$  mm<sup>3</sup> and two with dimensions of  $2 \times 2 \times 1$  mm<sup>3</sup>, were cut from a larger [001] plate ( $10 \times 10 \times 1$  mm<sup>3</sup>) provided by MTI. Fluorine was present in all the crystals supplied by MTI and, to our knowledge, was an unintentional contaminant. Its concentration level in our crystals, estimated from EPR, was less than one ppm by weight. The crystals received from MTI were colorless at room temperature and only exhibited EPR signals from  $\text{Fe}^{3+}$  and  $\text{Cr}^{3+}$  ions, thus indicating that they were fully oxidized. Subsequent reducing treatments in our laboratory consisted of placing a sample in flowing nitrogen gas while heating to high temperature.

A Bruker EMX spectrometer was used to take EPR data and a Bruker Elexsys E-500 spectrometer was used to take ENDOR data. These spectrometers operated near 9.47 GHz. Helium-gas-flow systems maintained the sample temperature in the 4–15 K range and proton NMR gaussmeters provided

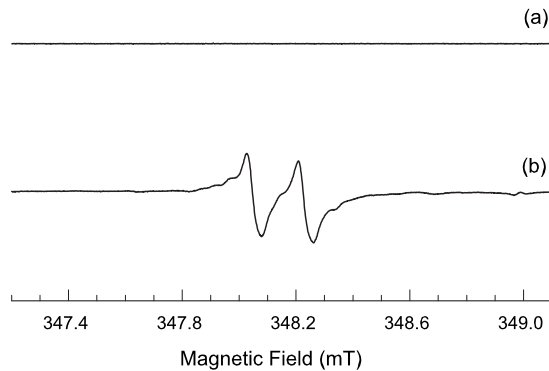


FIG. 1. EPR spectrum of the photoinduced neutral fluorine donor in a fully oxidized  $\text{TiO}_2$  (rutile) crystal. These data were taken at 6 K with the magnetic field along the  $[001]$  direction. (a) Spectrum taken in the dark after cooling in the dark (there is no signal). (b) Spectrum taken during exposure to 442 nm laser light.

values of the static magnetic field. A small Cr-doped MgO crystal was used to correct for the difference in magnetic field between the sample and the probe tips of the gaussmeters (the isotropic  $g$  value for  $\text{Cr}^{3+}$  in MgO is 1.9800). Narrow slots in the end of the Bruker  $\text{TE}_{102}$  rectangular microwave cavity allowed optical access to the sample. Approximately 15 mW of 442 nm light from a He-Cd laser was incident on the sample during the low-temperature illuminations.

### III. EPR RESULTS

Figure 1 shows the EPR doublet produced at 6 K in our fully oxidized  $3 \times 5 \times 1 \text{ mm}^3$   $\text{TiO}_2$  sample during exposure to 442 nm laser light. These spectra were taken with the magnetic field along the  $[001]$  direction. There were no EPR signals in this magnetic field region before illumination, as shown in Fig. 1(a). The photoinduced EPR doublet in Fig. 1(b) has a splitting of 0.180 mT and linewidths of 0.045 mT for this orientation of magnetic field. ENDOR experiments, described in Sec. IV, identify a hyperfine interaction with a  $^{19}\text{F}$  nucleus ( $I=1/2$ , 100% abundant) as the cause of the splitting. This, in turn, leads us to assign the EPR signal in Fig. 1(b) to a neutral fluorine donor.

We determined, with EPR, that trace amounts of  $\text{Fe}^{3+}$  and  $\text{Cr}^{3+}$  ions substitute for  $\text{Ti}^{4+}$  ions in our samples.<sup>16–18</sup> These trivalent transition-metal ions act as deep singly ionized acceptors and provide compensation for the singly ionized fluorine donors in the as-received crystals (i.e., one trivalent transition-metal ion charge compensates one  $\text{F}^-$  ion replacing an oxygen ion). Additional electronlike EPR signals appear in our fully oxidized samples during illumination at low temperature, including singly ionized oxygen vacancies, neutral oxygen vacancies,  $\text{Ti}^{3+}$ - $\text{Si}^{4+}$  centers, and  $\text{Ti}^{3+}$  self-trapped electrons.<sup>8</sup> Significant concentrations of self-trapped holes are also produced during illumination.<sup>8</sup> All of these EPR signals are easily saturated with microwave power at temperatures below 15 K and thus, although present, are not readily observed under the conditions used to obtain the spectra in Fig. 1. Self-trapped hole centers in  $\text{TiO}_2$  (rutile) consist of a

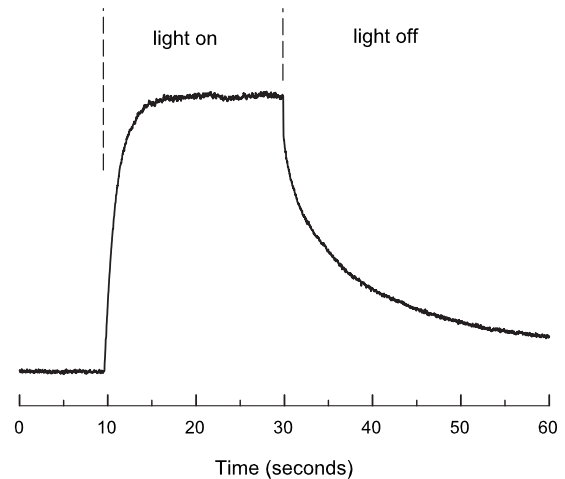


FIG. 2. Production and decay of the neutral fluorine donor EPR spectrum in a fully oxidized crystal as the 442 nm laser light was turned on and off. The monitoring temperature was 4.6 K.

hole localized on one or two oxygen ions in an otherwise perfect region of the crystal with lattice relaxation providing the trapping potential. These self-trapped hole centers are important in the present study as they are the source of the photoexcited electrons that temporarily convert the singly ionized fluorine donors to their neutral charge state at the very low temperatures. Monitoring the  $\text{Fe}^{3+}$  and  $\text{Cr}^{3+}$  EPR signals shows that they are not the primary source of electrons to form neutral fluorine donors when the temperature during illumination is below 15 K.

The production and thermal decay of the neutral fluorine donor in our fully oxidized  $3 \times 5 \times 1 \text{ mm}^3$  sample is illustrated in Fig. 2. These data were acquired by fixing the magnetic field at the peak of the derivative for one of the components of the fluorine doublet (see Fig. 1) and then monitoring the intensity of this EPR signal as a function of time while the 442 nm laser light was turned on and off. During this experiment, the temperature was maintained near 4.6 K and the magnetic field was along the  $[001]$  direction. The EPR signal reaches saturation within 5 s after the laser is turned on (the production rate depends on the incident laser power and the temperature). At 4.6 K, the EPR signal decays over tens of seconds when the laser is turned off and the sample is held in the dark. Raising the temperature slightly results in a faster decay of the EPR signal. At 7 K, the photoinduced EPR signal drops to a barely detectable level within a few seconds when the laser light is removed. We suggest that the rapid decay of the EPR signal in Fig. 2 occurs when holes are thermally released from the photoinduced self-trapped hole centers.<sup>8</sup> These thermally released holes move to the neutral fluorine donors and recombine with the trapped electrons, thus converting the neutral fluorine donors back to their singly ionized state. This release of holes in the dark at temperatures below 15 K is not a property of the fluorine donors in  $\text{TiO}_2$  and does not provide information about the ionization energy of these donors. Instead, the rapid decay of the neutral fluorine EPR signal at very low temperature indicates that the ionization energy of the self-trapped hole center is about 10–15 meV.

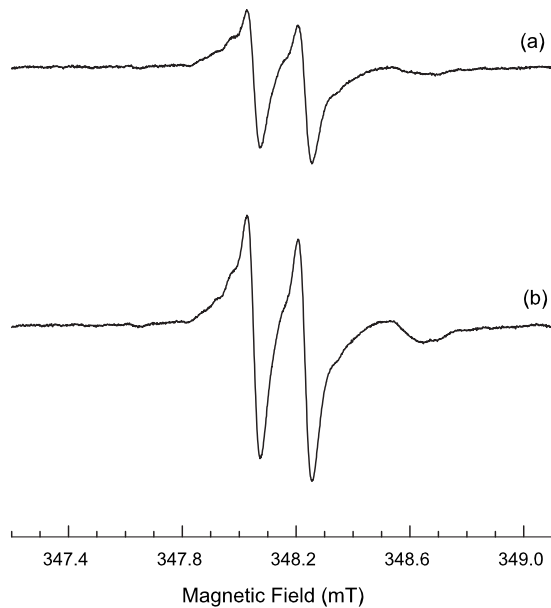


FIG. 3. EPR spectra taken at 6 K after reducing a TiO<sub>2</sub> crystal for 90 min at 600 °C in flowing nitrogen gas. The magnetic field was along the [001] direction. (a) Spectrum taken in the dark after cooling in the dark. (b) Spectrum taken during exposure to 442 nm laser light.

Following the characterization of the neutral fluorine EPR signals in the fully oxidized sample, one of the two smaller samples cut from the larger as-received TiO<sub>2</sub> plate was held at 600 °C for 90 min in flowing N<sub>2</sub> gas and then placed in the EPR spectrometer. The EPR signal from the neutral fluorine donor was easily observed in this reduced sample even though there was no light incident on the crystal during cooling or at low temperature prior to or during the time the spectrum was taken. These data are shown in Fig. 3(a) where the measuring temperature is 6 K and the magnetic field is along the [001] direction. The EPR signal became more intense when this sample was illuminated with 442 nm laser light while at 6 K, as shown in Fig. 3(b). A similar reducing treatment of the second smaller sample at 650 °C resulted in an even more intense fluorine EPR signal without light and there was no increase in the EPR signal when the sample was exposed to 442 nm light at 6 K. In general, heating in a nitrogen atmosphere introduces shallow donors (i.e., neutral oxygen vacancies), thus making the TiO<sub>2</sub> crystal more *n* type and significantly increasing the number of free carriers. At the low temperatures where we take EPR data, a portion of these electrons “freeze out” at the fluorine sites and produce the neutral fluorine donors that we observe with EPR in the absence of light. In other words, the reducing treatment raises the Fermi level and populates the neutral fluorine donors.

An interesting feature present in both spectra in Fig. 3 is the weak EPR signal near 348.6 mT (corresponding to an effective *g* value of 1.9408 when the magnetic field is parallel to the [001] direction). We also observe this EPR line in TiO<sub>2</sub> crystals that do not contain detectable amounts of fluorine donors. ENDOR spectra taken in our laboratory show that this EPR line at *g*=1.9408 when the magnetic field is

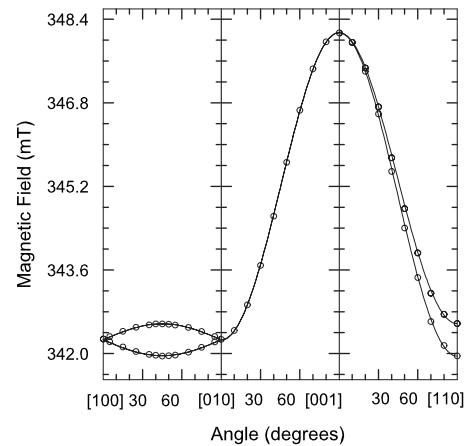


FIG. 4. Angular dependence of the *g* matrix for the neutral fluorine donor. These EPR data were acquired in the three high-symmetry planes using a reduced TiO<sub>2</sub> crystal. Single points at the centers of doublets are used for those angles where the fluorine hyperfine is resolved in the EPR spectra.

along the [001] direction has an unresolved hyperfine interaction with one hydrogen (*I*=1/2, nearly 100% abundant). We suggest that the responsible defect is a Ti<sup>3+</sup> ion adjacent to an OH<sup>-</sup> molecular ion (i.e., a neutral hydrogen donor in rutile-structured TiO<sub>2</sub>).

A complete angular dependence of the neutral fluorine donor EPR spectrum was taken at 6 K using the sample reduced at 600 °C for 90 min. As shown in Fig. 4, data were acquired in all three high-symmetry planes of the crystal. The sample was illuminated with 442 nm light during the measurements. These plots provide information about the principal values of the *g* matrix and the directions of the principal axes. The discrete points in Fig. 4 are experimental results and the solid curves are computer generated using the final set of “best” parameters for the *g* matrix. Fluorine hyperfine splittings are resolved in the EPR spectra for orientations of the magnetic field within approximately 60° of the [001] direction. At these angles, we have plotted the center positions of the resolved doublets. Thus, there is no hyperfine information in Fig. 4. The <sup>19</sup>F hyperfine matrix is analyzed in detail in Sec. IV. For completeness, we note that the low-field EPR line during the rotation from [001] to [110] in Fig. 4 has the larger fluorine hyperfine splitting.

The following spin Hamiltonian, expressed as a 2 × 2 matrix, was used to determine the parameters describing the angular-dependence data in Fig. 4:

$$\mathbf{H} = \beta \mathbf{S} \cdot \mathbf{g} \cdot \mathbf{B}. \quad (1)$$

Only two crystallographically equivalent sites are required to explain the *g* matrix angular-dependence patterns in Fig. 4 (in contrast, four crystallographically equivalent sites are required to explain the angular dependence of the higher-resolution fluorine ENDOR spectra in Sec. IV). In Fig. 4, the two sites are magnetically equivalent when rotating from [010] to [001] and are magnetically inequivalent when rotating in the other two planes. The two resolved sites are associated with the two equivalent distorted TiO<sub>6</sub> octahedra that

TABLE I. Spin-Hamiltonian parameters for one site of the neutral fluorine donor in a TiO<sub>2</sub> (rutile) crystal. The principal axes associated with  $g_1$  and  $A_1$  are parallel to the elongation direction of the distorted TiO<sub>6</sub> octahedron (specified to be [110] for the site described below). Directions of the principal axes for  $A_2$  and  $A_3$  are in the (110) plane (see the model in Fig. 7). The uncertainty in the directions of principal axes is  $\pm 1^\circ$ .

	Principal value	Principal-axis direction
$g$ matrix		
$g_1$	$1.9746 \pm 0.0001$	[110]
$g_2$	$1.9782 \pm 0.0001$	$[\bar{1}10]$
$g_3$	$1.9430 \pm 0.0001$	[001]
$^{19}\text{F}$ hyperfine matrix		
$A_1$	$-0.23 \pm 0.01$ MHz	[110]
$A_2$	$0.47 \pm 0.01$ MHz	$13.8^\circ$ from $[\bar{1}10]$
$A_3$	$5.15 \pm 0.01$ MHz	$13.8^\circ$ from [001]

are present in the TiO<sub>2</sub> (rutile) lattice. These two TiO<sub>6</sub> units are elongated in directions perpendicular to the [001] direction with the six oxygen ions separating into a set of two along the elongation direction and a set of four perpendicular to the elongation direction. The two octahedra are related by a 90° rotation about the [001] direction. Figure 4 shows that the directions of the principal axes of the  $g$  matrix for the fluorine donor are along (or very near) high-symmetry directions in the crystal. Principal values of 1.9746, 1.9782, and 1.9430 are obtained from the magnetic fields measured at the turning points in Fig. 4, i.e., the two turning points at [110] and  $[\bar{1}10]$  and the one turning point at [001]. The principal axis associated with the 1.9430 principal value is along the [001] direction in the crystal. Our ENDOR results in Sec. IV show that the principal axis associated with the 1.9746 principal value is along the elongation direction containing the two equivalent oxygen ions in a TiO<sub>6</sub> octahedron. We specify the elongation direction of this octahedron as [110]. The principal values and the directions of the principal axes for the  $g$  matrix at one site are summarized in Table I. Our model for the neutral fluorine donor, presented in Sec. V, does not require principal axes of the  $g$  matrix to be along the [001] and  $[\bar{1}10]$  directions. However, the lack of additional splittings in our EPR angular dependence, other than those shown in Fig. 4, places an upper limit on the deviations of these  $g$ -matrix principal axes from the high-symmetry directions. Taking into account our EPR linewidths, we estimate that the uncertainties in the principal-axis directions of the  $g$  matrix in Table I are less than  $1^\circ$ . Future studies, where EPR spectra are taken at higher microwave frequencies, may help determine if the principal-axis directions of the  $g$  matrix are exactly along the high-symmetry directions in the crystal or whether they deviate slightly from these directions.

#### IV. ENDOR RESULTS

The [001] ENDOR spectrum of the neutral fluorine donor is shown in Fig. 5. These data were taken at 5 K from the

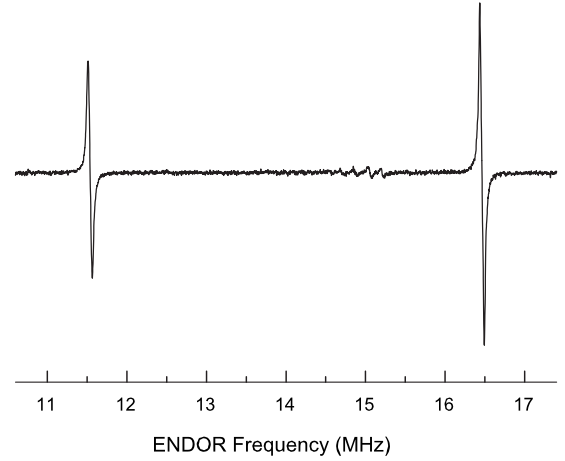


FIG. 5. ENDOR spectrum from the neutral fluorine donor in a reduced TiO<sub>2</sub> crystal. Data were taken at 5 K with the magnetic field parallel to the [001] direction. The weak signals near 15 MHz are due to protons associated with the hydrogen-related donor discussed in Sec. III.

sample that had been reduced at 650 °C. This choice of sample eliminated the need to use the 442 nm laser light at low temperature to maximize the fluorine donor EPR signal. The two lines in Fig. 5 are separated by 4.915 MHz and are centered on 13.986 MHz. Their linewidths are 55 kHz. For a weak hyperfine interaction, the first-order ENDOR spectrum from an  $I=1/2$  nucleus consists of two lines separated by the hyperfine parameter  $A$  and centered on the “free” nuclear-spin frequency  $\nu_N$  (where  $\nu_N = g_N \beta_N H / h$ ). The ENDOR spectrum in Fig. 5 was taken at a magnetic field of 348.724 mT and the corresponding value of  $\nu_N$  for a  $^{19}\text{F}$  nucleus is 13.976 MHz (values of  $\nu_N$  for all nuclei are tabulated in Appendix A of Ref. 19). This known value of  $\nu_N$  for  $^{19}\text{F}$  is very close to the experimental value for the center of the two lines in Fig. 5 and thus conclusively shows that a  $^{19}\text{F}$  nucleus is responsible for the hyperfine splitting observed in the [001] EPR spectrum.

Figure 6 shows the angular dependence of the  $^{19}\text{F}$  EN-

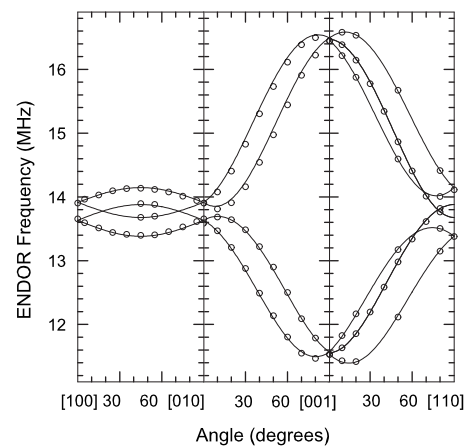


FIG. 6. Angular dependence of the hyperfine matrix for the neutral fluorine donor. These ENDOR data were acquired in the three high-symmetry planes using a reduced TiO<sub>2</sub> crystal.

DOR spectrum. Results from all three high-symmetry planes are included. The discrete points are experimental data taken at 5 K with no illumination and the solid curves are computer generated using the final set of best parameters. Four crystallographically equivalent sites are needed to describe the  $^{19}\text{F}$  hyperfine matrix. Two of these sites are associated with one distorted  $\text{TiO}_6$  octahedron and two are associated with the second distorted  $\text{TiO}_6$  octahedron generated from the first by a  $90^\circ$  rotation about the  $[001]$  direction. As shown in Fig. 6, the four sites are pairwise magnetically equivalent when the magnetic field is rotated from  $[100]$  to  $[010]$  and from  $[010]$  to  $[001]$ . The four sites divide into three sets (with degeneracies of one, two, and one) when rotating the magnetic field from  $[001]$  to  $[110]$ . Along the  $[110]$  direction of magnetic field in Fig. 6, the outer pair of ENDOR lines at 13.38 and 14.14 MHz are obtained from the EPR line at 343.39 mT while the inner pair of ENDOR lines at 13.68 and 13.89 MHz are obtained from the EPR line at 344.01 mT. This inner pair of ENDOR lines comes from the two sites that are magnetically equivalent when the magnetic field is rotated from  $[001]$  to  $[110]$ .

The following spin Hamiltonian, with electron Zeeman, hyperfine, and nuclear Zeeman terms, was used to analyze the angular-dependence data in Fig. 6:

$$\mathbf{H} = \beta\mathbf{S} \cdot \mathbf{g} \cdot \mathbf{B} + \mathbf{I} \cdot \mathbf{A} \cdot \mathbf{S} - g_N\beta_N\mathbf{I} \cdot \mathbf{B}. \quad (2)$$

Final values for the hyperfine parameters were obtained from a least-squares fitting procedure that involved exact diagonalizations of the  $4 \times 4$  Hamiltonian matrix ( $S=1/2, I=1/2$ ). The computer programs used to fit our EPR and ENDOR angular-dependence data were developed in house. When fitting the ENDOR data, the  $g$  matrix was fixed at the values and directions given in Table I. From the data in Fig. 6, one of the principal axes of the  $^{19}\text{F}$  hyperfine matrix must be along the  $[110]$  direction. Specifically, we find that the 1.9746 principal  $g$  value and the  $-0.23$  MHz principal hyperfine value have principal axes along the  $[110]$  direction (i.e., the elongation direction containing the two equivalent oxygen ions in a distorted  $\text{TiO}_6$  octahedron). Turning points in Fig. 6 indicate that the remaining two hyperfine principal axes are not along high-symmetry directions of the crystal. These principal axes must, however, be in the  $(110)$  plane and one angle suffices to define their directions. Thus, during the ENDOR fitting process, only four parameters were varied (three principal values and one angle). Results obtained from fitting the experimental data in Fig. 6 are listed for one site in Table I.

## V. DISCUSSION

Fluorine ions substitute for oxygen ions in  $\text{TiO}_2$  (rutile) and form shallow donors. All of the fluorine donors are in the singly ionized charge state (with no unpaired spins and thus no EPR signal) in fully oxidized crystals cooled in the dark when a sufficient number of deep transition-metal-ion acceptors are present to provide compensation. Photoexcited electrons produced during an illumination at very low temperature convert a portion of these fluorine donors to the neutral charge state which is EPR active. However, unlike a classic

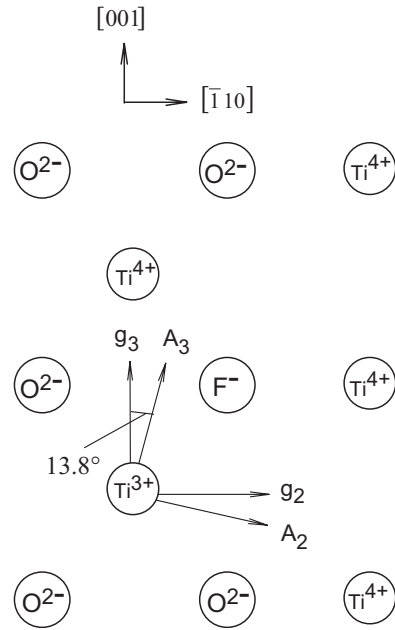


FIG. 7. Model of the neutral fluorine donor illustrating the localization of the unpaired electron on a neighboring titanium ion. This is a projection on the  $(110)$  plane. The  $g_1$  and  $A_1$  principal axes are along the  $[110]$  direction.

donor, the unpaired electron associated with the neutral charge state of the fluorine donor is not centered on the fluorine ion in a hydrogenlike wave function that spreads out over many shells of neighboring ions and reflects the symmetry of the lattice. Instead, we find that the unpaired electron is localized, to a first approximation, on one titanium ion immediately adjacent to the fluorine ion. In other words, it is energetically more favorable to have the “extra” electron in a  $d$  orbital on the titanium ion than delocalized in an effective-mass (i.e., hydrogenlike) wave function centered on the fluorine ion.

Our primary evidence for a  $\text{Ti}^{3+}$  model for the neutral fluorine donor comes from the fluorine hyperfine matrix. Table I shows that the  $^{19}\text{F}$  matrix has significant anisotropy, with the principal axis associated with the largest principal value (5.15 MHz) deviating  $13.8^\circ$  from the  $[001]$  direction. If a hydrogenic model for the fluorine donor were correct, then all of the principal axes of the fluorine hyperfine matrix would be along high-symmetry directions in the crystal and the anisotropy would be minimal. A model for the neutral fluorine donor is shown in Fig. 7, including principal axes of the  $g$  and  $^{19}\text{F}$  hyperfine matrices. A substitutional fluorine ion in  $\text{TiO}_2$  has three nearest-neighbor titanium ions. The two neighboring titanium ions along the  $[001]$  direction are equivalent and they are closer to the fluorine ion than the remaining titanium ion along the  $[\bar{1}10]$  direction. In the regular  $\text{TiO}_2$  lattice at room temperature, these Ti-O distances are 1.9485 and 1.9800 Å, respectively.<sup>20</sup> As we show in Fig. 7, the neutral fluorine donor has the electron localized on one of these two titanium ions along the  $[001]$  direction. The Coulomb energy is minimized in this configuration. If the electron was localized on the slightly more distant titanium ion along the  $[\bar{1}10]$  direction, this Coulomb energy would be

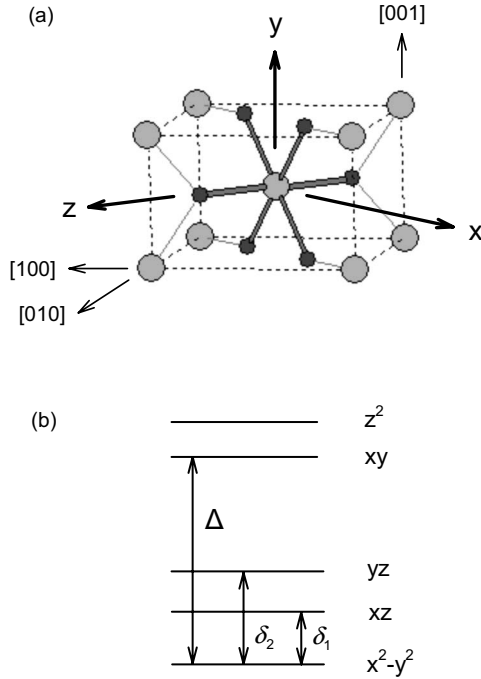


FIG. 8. (a) Distorted TiO<sub>6</sub> octahedron (the center ion is the Ti<sup>3+</sup> ion, the six smaller dark solid circles are oxygen ions, and the eight larger shaded circles are Ti<sup>4+</sup> ions). The  $x$ ,  $y$ , and  $z$  coordinate system is used in the  $g$  matrix analysis. (b) Energy ordering of the five  $d$  orbitals.

higher and, more importantly, the <sup>19</sup>F hyperfine matrix would not exhibit the observed 13.8° angle.

The measured  $g$  matrix is also consistent with our model of a substitutional Ti<sup>3+</sup> ion next to an F<sup>-</sup> ion. The EPR and ENDOR angular-dependence data in Figs. 4 and 6 and the parameters in Table I show that the two principal-axis directions of the  $g$  matrix in the (110) plane are along (or very near) the [001] and  $[\bar{1}10]$  high-symmetry directions, and thus differ considerably from the two corresponding principal-axis directions of the fluorine hyperfine matrix. This is consistent with the expectation that the  $d$  orbitals on the Ti<sup>3+</sup> ion will not be strongly perturbed by the presence of the neighboring fluorine ion and allows us to derive simple expressions for the principal values of the  $g$  matrix. Figure 8(a) shows one of the two equivalent distorted TiO<sub>6</sub> octahedra in the TiO<sub>2</sub> (rutile) lattice. The Ti<sup>3+</sup> ion is at the center and the six neighboring oxygen ions are represented by the dark solid circles. We consider the case when six oxygen ions are present (replacing one of the four equivalent oxygen ions in the (110) plane with a fluorine does not change our analysis). The  $x$ ,  $y$ , and  $z$  coordinate system in Fig. 8(a) has  $x$  along the  $[\bar{1}10]$  direction,  $y$  along the [001] direction, and  $z$  along the [110] direction. The five  $d$  orbitals can be written as

$$|xy\rangle = -\frac{i}{\sqrt{2}}(|2,2\rangle - |2,-2\rangle), \quad (3)$$

$$|xz\rangle = \frac{1}{\sqrt{2}}(|2,-1\rangle - |2,1\rangle), \quad (4)$$

$$|yz\rangle = \frac{i}{\sqrt{2}}(|2,-1\rangle + |2,1\rangle), \quad (5)$$

$$|x^2-y^2\rangle = \frac{1}{\sqrt{2}}(|2,2\rangle + |2,-2\rangle), \quad (6)$$

$$|z^2\rangle = |2,0\rangle. \quad (7)$$

Note that the  $x$  and  $y$  axes do not point toward the nearest-neighbor negative ions in Fig. 8(a). The choice of coordinate system and the positions of the nearest-neighbor negative ions in Fig. 8(a) produce the relative energy ordering shown in Fig. 8(b) for these five  $d$  orbitals ( $|x^2-y^2\rangle$  is lowest in energy and  $|z^2\rangle$  is highest in energy). As described by Kasai,<sup>21</sup> the  $|x^2-y^2\rangle$  orbital is lowest in energy because of two nearest-neighbor Ti<sup>4+</sup> ions along the [001] direction, one above and one below the Ti<sup>3+</sup> ion. The  $g$  matrix for a  $d^1$  electron is then given, to first order, by the following expressions:<sup>22</sup>

$$\mathbf{g} = g_e \hat{\mathbf{1}} + 2\lambda \hat{\Lambda} \quad \text{where} \quad \Lambda_{ij} = -\sum_{n \neq G} \frac{\langle G|L_i|n\rangle \langle n|L_j|G\rangle}{E_n - E_G}. \quad (8)$$

The equation for  $\Lambda_{ij}$  involves matrix elements of the orbital momentum operators  $L_i$  ( $i=x, y$ , and  $z$ ) between the ground state  $G$ , with energy  $E_G$ , and the four higher states  $n$ , with energies  $E_n$ . Evaluating these matrix elements leads us to the principal values of the  $g$  matrix,

$$g_x = g_e - \frac{2\lambda}{\delta_2}, \quad g_y = g_e - \frac{2\lambda}{\delta_1}, \quad g_z = g_e - \frac{8\lambda}{\Delta}. \quad (9)$$

The energy differences  $\delta_1$ ,  $\delta_2$ , and  $\Delta$  are defined in Fig. 8(b). In Eq. (9),  $g_e = 2.0023$  and  $\lambda$  is the spin-orbit coupling constant (+154 cm<sup>-1</sup> for a free Ti<sup>3+</sup> ion). To partially account for covalency, an orbital reduction factor  $k$  is introduced that reduces the spin-orbit constant ( $\lambda' = k\lambda$ ). We take  $k$  to be 0.6, thus making  $\lambda' = 92.4$  cm<sup>-1</sup>. The measured  $g_1$ ,  $g_2$ , and  $g_3$  values in Table I correspond to  $g_z$ ,  $g_x$ , and  $g_y$ , respectively. Substituting these measured  $g$  values into Eq. (9) and replacing  $\lambda$  with  $\lambda'$  gives  $\delta_1 = 3120$  cm<sup>-1</sup>,  $\delta_2 = 7670$  cm<sup>-1</sup>, and  $\Delta = 26\,700$  cm<sup>-1</sup>. A cursory examination of the measured principal  $g$  values in Table I suggests that the  $g$  matrix is very nearly axial. Our analysis, however, verifies the orthorhombic nature of the titanium site and shows that a fortuitous splitting of the  $d$  levels causes  $g_1$  and  $g_2$  to have similar values.

An additional source of evidence to support a Ti<sup>3+</sup> model would be resolved hyperfine lines from <sup>47</sup>Ti and <sup>49</sup>Ti nuclei. Unfortunately, information of this type is not available from our EPR spectra. The signal-to-noise ratios of the EPR signals in Figs. 1 and 3 are not large enough to permit an unambiguous identification of surrounding <sup>47</sup>Ti and <sup>49</sup>Ti lines (these hyperfine lines will be at least 46 times smaller than the central pair of fluorine lines). As a further complication, weak EPR signals from unidentified point defects are also present in this magnetic field region and may overlap the <sup>47</sup>Ti and <sup>49</sup>Ti lines. We expect that TiO<sub>2</sub> crystals containing

larger concentrations of fluorine ions will provided detailed information about the <sup>47</sup>Ti and <sup>49</sup>Ti hyperfine interactions.

## VI. SUMMARY

A detailed EPR and ENDOR study of the neutral fluorine donor in TiO<sub>2</sub> (rutile) bulk crystals is reported. These neutral donors, along with self-trapped hole centers, are produced in fully oxidized crystals by illumination with below-band-gap laser light (442 nm) at low temperature (10 K and below). The EPR signals from these defects quickly decay at the low temperatures when the light is removed, as holes thermally release from the self-trapped hole centers and recombine with electrons trapped at the fluorine ions. Reducing a TiO<sub>2</sub> crystal at high temperature in a nitrogen atmosphere intro-

duces neutral oxygen-vacancy donors that raise the Fermi level and populate the neutral fluorine donors. In the reduced crystal, electrons are available from these oxygen vacancies to form the neutral fluorine donors and photoexcitation is not needed. From the angular dependences of the EPR and ENDOR spectra, we determine that the neutral fluorine donor in TiO<sub>2</sub> consists of a substitutional Ti<sup>3+</sup> ion adjacent to a F<sup>-</sup> ion substituting for an oxygen ion. Our analysis of the principal values of the *g* matrix suggests that the unpaired *d* electron on the Ti<sup>3+</sup> ion occupies a  $|x^2-y^2\rangle$  orbital.

## ACKNOWLEDGMENT

This research was supported by Grant No. DMR-0804352 from the National Science Foundation.

\*Corresponding author; larry.halliburton@mail.wvu.edu

- <sup>1</sup>F. A. Grant, *Rev. Mod. Phys.* **31**, 646 (1959).
- <sup>2</sup>X. Chen and S. S. Mao, *Chem. Rev. (Washington, D.C.)* **107**, 2891 (2007).
- <sup>3</sup>A. Fujishima, X. Zhang, and D. A. Tryk, *Surf. Sci. Rep.* **63**, 515 (2008).
- <sup>4</sup>C. L. Pang, R. Lindsay, and G. Thornton, *Chem. Soc. Rev.* **37**, 2328 (2008).
- <sup>5</sup>A. Ghicov and P. Schmuki, *Chem. Commun. (Cambridge)* **2009**, 2791.
- <sup>6</sup>K. Shankar, J. I. Basham, N. K. Allam, O. K. Varghese, G. K. Mor, X. Feng, M. Paulose, J. A. Seabold, K. S. Choi, and C. A. Grimes, *J. Phys. Chem. C* **113**, 6327 (2009).
- <sup>7</sup>J.-M. Spaeth and H. Overhof, *Point Defects in Semiconductors and Insulators: Determination of Atomic and Electronic Structure from Paramagnetic Hyperfine Interactions*, Springer Series of Materials Science Vol. 51 (Springer-Verlag, Berlin, 2003).
- <sup>8</sup>Shan Yang, L. E. Halliburton, A. Manivannan, P. H. Bunton, D. B. Baker, M. Klemm, S. Horn, and A. Fujishima, *Appl. Phys. Lett.* **94**, 162114 (2009).
- <sup>9</sup>H. J. Meng, D. L. Hou, L. Y. Jia, X. J. Ye, H. J. Zhou, and X. L. Li, *J. Appl. Phys.* **102**, 073905 (2007).
- <sup>10</sup>Q. Zhao, P. Wu, B. L. Li, Z. M. Lu, and E. Y. Jiang, *J. Appl. Phys.* **104**, 073911 (2008).
- <sup>11</sup>S. Zhou, E. Cizmar, K. Potzger, M. Krause, G. Talut, M. Helm, J. Fassbender, S. A. Zvyagin, J. Wosnitza, and H. Schmidt, *Phys. Rev. B* **79**, 113201 (2009).
- <sup>12</sup>J. C. Yu, J. Yu, W. Ho, Z. Jiang, and L. Zhang, *Chem. Mater.* **14**, 3808 (2002).
- <sup>13</sup>A. M. Czoska, S. Livraghi, M. Chiesa, E. Giamello, S. Agnoli, G. Granozzi, E. Finazzi, C. Di Valentin, and G. Pacchioni, *J. Phys. Chem. C* **112**, 8951 (2008).
- <sup>14</sup>C. Di Valentin, E. Finazzi, G. Pacchioni, A. Selloni, S. Livraghi, A. M. Czoska, M. C. Paganini, and E. Giamello, *Chem. Mater.* **20**, 3706 (2008).
- <sup>15</sup>Q. Wang, C. Chen, W. Ma, H. Zhu, and J. Zhao, *Chemistry (Weinheim, Ger.)* **15**, 4765 (2009).
- <sup>16</sup>H. J. Gerritsen, S. E. Harrison, H. R. Lewis, and J. P. Wittke, *Phys. Rev. Lett.* **2**, 153 (1959).
- <sup>17</sup>D. L. Carter and A. Okaya, *Phys. Rev.* **118**, 1485 (1960).
- <sup>18</sup>G. J. Lichtenberger and J. R. Addison, *Phys. Rev.* **184**, 381 (1969).
- <sup>19</sup>J.-M. Spaeth, J. R. Niklas, and R. H. Bartram, *Structural Analysis of Point Defects in Solids: An Introduction to Multiple Magnetic Resonance Spectroscopy*, Springer Series in Solid-State Sciences Vol. 43 (Springer-Verlag, Berlin, 1992).
- <sup>20</sup>S. C. Abrahams and J. L. Bernstein, *J. Chem. Phys.* **55**, 3206 (1971).
- <sup>21</sup>P. H. Kasai, *Phys. Lett.* **7**, 5 (1963).
- <sup>22</sup>J. E. Wertz and J. R. Bolton, *Electron Spin Resonance: Elementary Theory and Practical Applications* (McGraw-Hill, New York, 1972), pp. 278–281.